Chapter 11
Numerical Simulation Analysis of Dynamic Response and Damage Effect of Tunnel Under Internal Explosion

Xiang Liu, Yuxin Sun, and Rongjun Guo

Abstract An investigation on dynamic response of explosion shock wave in different tunnel structure was carried out in this paper. Straight tunnel, L-shaped tunnel and T-shaped tunnel were selected as the research objects. And simulations were conducted with 2-D fluid–structure coupled model using the AUTODYN 19.0 software. Here, the RHT model was adopted to describe the mechanical behaviour of concrete and rock, and JWL equation of state was selected for explosive. Combined with the simulation results, the propagation law of shock wave in different tunnels was analysed, and the vulnerable points in the tunnel under the action of explosion shock wave were found. The results show that the damage of tunnel caused by explosion load was mainly concentrated in a very short time after explosion. And the dynamic response has the characteristics of fast response, large load and short duration. The explosion shock wave caused great damage to the tunnel structure which was close to the burst point. At the same time, the concentrated load was generated in the corner of the tunnel, which became a vulnerable structure.

11.1 Introduction

Tunnel is an engineering building buried in the ground, which is a form of human using underground space. In wartime, it can play the functions of civil air defense evacuation, transportation reserve materials, personnel emergency shelter and so on. With the development of weapons and guidance technology in modern war, the possibility of explosion in tunnel is increasing. When the explosion occurs in the tunnel structure, the explosion load has a direct or indirect impact on the tunnel's wall and the surrounding rock outside the tunnel. Therefore, it is very important to analyze the dynamic response and damage effect of the tunnel structure under the load of explosion in the tunnel, which is the basis of the anti-explosion performance evaluation and protection design of the tunnel structure.

X. Liu · Y. Sun (✉) · R. Guo
National Key Laboratory of Transient Physics, Nanjing University of Science and Technology, Jiangsu 210094, China
e-mail: yxsun01@163.com

A. Gany and X. Fu (eds.), *2021 International Conference on Development and Application of Carbon Nanomaterials in Energetic Materials*, Springer Proceedings in Physics 276,
https://doi.org/10.1007/978-981-19-1774-5_11

There is a significant difference between the propagation of explosion shock wave in closed space and that in open three-dimensional space. Due to the tunnel structure is not easy to build and the cost is huge, the methods of model test and numerical simulation are generally used. Benselama [1] and Uystpruyst [2] pointed out that there are two modes of propagation of explosion shock wave in the roadway: one is free propagation in three-dimensional space near the burst point, and the other is quasi one-dimensional propagation far away from the burst point. The relationship between the two modes of transfer position, explosive quantity and geometry of the propagation space was proposed by numerical calculation; Alex and Michael [3] studied the propagation behavior of explosion shock waves in underground mines through a series of experiments in experimental mines. A simple proportional relationship between peak overpressure and explosive quantity and propagation space was established. Kezhi and Xiumin [4] used the three-dimensional numerical simulation program to calculate the chemical explosion flow field in the long tunnel, and compared with the experimental results. The propagation law of air shock wave along tunnel direction was concluded; Pang et al. [5] established a formula to predict the air shock wave of high explosive explosion in tunnel through experiments; Xinjian et al. [6] mapped the velocity model of shock wave propagating along a straight tunnel with equal cross section under the condition of internal explosion at the entrance of the tunnel through experiments.

For the current research of explosion in tunnel, the focus is mainly on the propagation law of explosion shock wave, which was quite complete. However, these studies generally regard the tunnel as a non-deformable structure, ignoring the dynamic response and damage of tunnel structure under the action of shock wave.

Therefore, this paper intends to carry out numerical simulation for three typical tunnel structures to analyze the dynamic response and damage effect of tunnel structure under the load of internal explosion.

11.2 Numerical Simulation Model

11.2.1 AUTODYN Software

In order to solve highly nonlinear dynamic problems, such as solid, liquid, gas and their interactions, century dynamics Inc. has developed a nonlinear dynamic analysis software AUTODYN. The company first launched a two-dimensional version of autodyn-2D in 1986 and a three-dimensional software autodyn-3D in 1991. In January 2005, AUTODYN software was acquired by ANSYS company and has been integrated into ANSYS co-simulation platform. In the past few decades, autodyn-2D/3D software has been continuously developed, with increasingly perfect functions and more convenient application. Since its development, the software has been committed to the research and development of the military industry, and has become one of the most famous numerical simulation software in the field of explosive

mechanics and high-speed collision in the world. It integrates a variety of processing technologies of finite difference, computational fluid dynamics and fluid coding, and can be widely used in various complex engineering problems, such as large strain and large deformation, Nonlinear dynamics, explosion penetration, collision and fluid solid coupling shorten the development cycle of many products. There are many material constitutive models and equations of state, which are convenient for their application in various aspects. AUTODYN version 19.0 was used in this paper.

11.2.2 Research Objects

This paper discussed three kinds of tunnel structure. Straight tunnel, L-shaped tunnel and T-shaped tunnel were selected to establish two-dimensional simulation model for numerical simulation. The concrete wall thickness of three kinds of tunnel is 0.02 m, and the thickness of surrounding rock outside the tunnel is 0.5 m. Among them, the straight tunnel's burst points are distributed in the vertical direction; the L-shaped tunnel's burst points are distributed along the diagonal of the corner; the T-shaped tunnel burst points are also distributed in the vertical direction. The tunnel structure, location of burst points and observation points are shown in Figs. 11.1 and 11.2.

A 0.5 kg spherical COMP B was used in the simulation. The concrete wall and rock use Lagrange element, the COMP B and air use Euler element. The fluid structure coupling relationship between them was established.

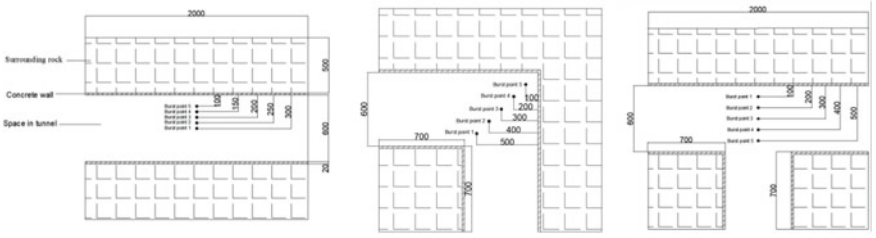

(a1) Straight tunnel (b1) L -shape tunnel (c1) T-shape tunnel

Fig. 11.1 Location of burst points in tunnels

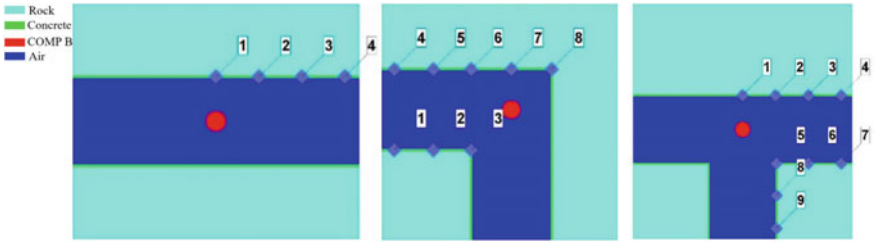

(a1) Straight tunnel (b1) L-shape tunnel (c1) T-shape tunnel

Fig. 11.2 Location of observation point in tunnels

11.2.3 Material Model

11.2.3.1 Concrete and Rock

Rock and concrete are both brittle materials, which have similar grain boundaries, holes, cracks and other defects of different sizes. Both of them have the characteristics of strain hardening, damage softening and strain rate effect, which provides the feasibility for us to use the constitutive relationship of concrete to describe the mechanical behavior of rock like brittle materials under dynamic and static loads. RHT concrete constitutive model has been widely used in the numerical simulation and analysis of explosion, impact, penetration and other problems, and achieved relatively satisfactory results.

The P-alpha EOS and RHT strength parameters of concrete and rock are mainly referred to [3, 4], and the main parameters are shown in Table 11.1.

11.2.3.2 COMP B

JWL equation of state was selected for explosive

$$p = A\left(1 - \frac{\omega}{R_1\overline{V}}\right)e^{-R_1\overline{V}} + B\left(1 - \frac{\omega}{R_2\overline{V}}\right)e^{-R_2\overline{V}} + \frac{\omega}{\overline{V}}E$$

where, A and B are the linear coefficient; R_1, R_2, ω are the non-linear coefficient; $\overline{V} = V_i/V_0$, V_i is volume of detonation product, V_0 is volume of unexploded explosive. A, B, R_1, R_2, ω are constants, which are obtained from experiments. The parameters are shown in Table 11.2.

Table 11.1 RHT model parameters of concrete and rock

Parameter	Concrete	Rock
(a) *P-alpha EOS*		
Initial density ρ_0(g/cm^3)	2.75	2.7
Pore density ρ_1(g/cm^3)	2.314	2.314
Initial pressure P_1(KPa)	2.33×10^4	2.33×10^4
Compaction pressure P_2(KPa)	6×10^6	6×10^6
Porosity index N	3	3
A_1 (KPa)	3.53×10^7	4.54×10^7
A_2 (KPa)	3.96×10^7	4.19×10^7
KPa)	9.04×10^6	4.20×10^6
B_0	1.22	0.9
B_1	1.22	0.9
T_1 (KPa)	3.53×10^7	4.54×10^7
T_2 (KPa)	0	0
(b) *RHT Strength model*		
Shear modulus G (KPa)	1.67×10^7	1.67×10^7
Compressive strength f_c (KPa)	3.5×10^4	4.8×10^4
Tension strength f_t/f_c	0.1	0.1
Shear strength f_s/f_c	0.18	0.18
Intact failure surface constant A	1.6	1.6
Intact failure surface exponent N	0.61	0.61
Tens./Comp. Meridian ratio Q	0.7	0.6805
Brittle to Ductile Transition BQ	0.0105	0.0105
Hardening slope	2.0	0.5
Elastic strength/ft	0.7	0.7
Elastic strength/fc	0.53	0.53
Fracture strength constant B_{fric}	1.6	1.6
Fracture strength exponent n_{fric}	0.61	0.61
Strain rate exponent α	0.032	0.02439
Tensile strain rate exponent β	0.036	0.02941

11.2.3.3 Air

The material model of air is assumed to be an ideal gas, and the relationship between pressure P and energy E can be determined by the following formula:

$$P = (k-1)\rho E$$

where, k is the adiabatic coefficient of gas, ρ is the density of air, E is the initial internal energy of air. The specific parameters are shown in Table 11.3.

Table 11.2 JWL model parameters of explosive materials

Parameter	Value
Density $\rho(\mathrm{g/cm^3})$	1.717
Detonation velocity D (m/s)	7980
C-J explosion pressure P (Pa)	2.95×10^{10}
Material constant A (Pa)	5.2423×10^{11}
Material constant B (Pa)	7.678×10^{9}
Material constant R_1	4.2
Material constant R_2	1.1
Material constant ω	0.34
Initial internal energy $E_0(\mathrm{J/m^3})$	8.5×10^{9}

Table 11.3 Ideal gas model parameters of air

Parameter	Value
Density $\rho(\mathrm{g/cm})^3$	1.225×10^{-3}
Internal energy $(\mathrm{mJ/mm^3})$	2.068×10^{5}
Isentropic adiabatic coefficient	1.4

11.3 Calculation Results and Analysis

11.3.1 Straight Tunnel

Figures 11.3 and 11.4 show the stress distributing graph and crack propagation process of tunnel structure under the action of explosion in straight tunnel. A strong shock wave was formed after the explosion, and the tunnel structure near the burst point was the first to be impacted and deformed. When T = 0.3 ms, stress concentration occurred, and some materials of tunnel structure enter the plastic stage. When the stress intensity was higher than the material strength, the material damage forms cracks, and the cracks were mainly concentrated near the burst point. The crack propagation at T = 5 ms was almost the same as that at T = 0.5 ms, which indicated that the material was damaged mainly in the short time at the beginning of explosion.

Figure 11.5 shows the dynamic response observed at observation points 1–4 after the explosion at burst point 1 in the straight tunnel. Observation points 1–4 are 0.3 m away from the explosion point in the Y direction, and 0, 0.3, 0.6 and 0.9 m away from the burst point in the X direction. The maximum stress of Observation points 1–4 were 80.44, 37.23, 17.51 and 14.24 MPa. The maximum strain of Observation points 1–4 were 0.029, 0.013, 0.0075 and 0.0067. In the X direction, the closer the wall structure is to the burst point, the greater the maximum stress and strain was observed. The displacement and the maximum acceleration had similar law.

Figure 11.6 is the dynamic response curve observed at observation points 1 after the explosion of different burst points. In Fig. 11.6a, the stress at burst point 5 decreased rapidly to 0 MPa after reached the maximum value of about 350 MPa.

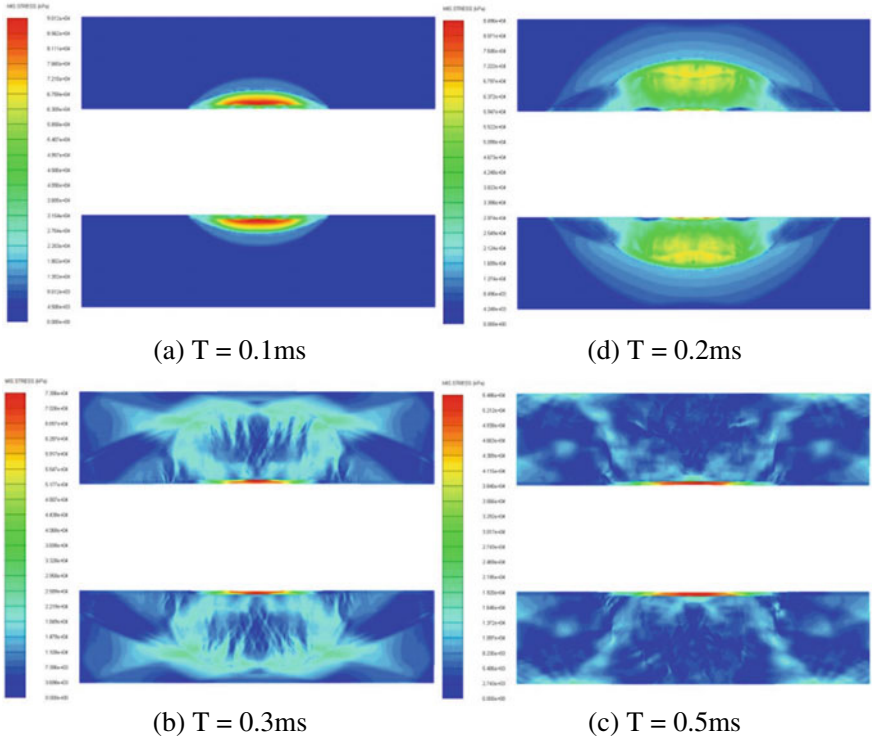

Fig. 11.3 Stress distributing graph after the explosion of burst point 3 in the straight tunnel

Which was a clear manifestation of that the structure had failed, and the failed structure couldn't bear any tensile stress anymore. In Fig. 11.6b, the maximum strains under the load of exploration which happened at burst points 1–5 were 0.028, 0.039, 0.047, 0.084 and 0.217. The closer the burst point was to the tunnel wall, the greater the maximum strain of tunnel wall structure. The stress, displacement and maximum acceleration have similar law.

In Fig. 11.6d, the response times observed at observation point 1 were 0.05, 0.03, 0.02, 0.01 and 0.003 ms. The speed increased rapidly to tens or hundreds of meters per second, and decreased to about 0 ms at 0.3 ms. The dynamic response is very fast, reaching microsecond level, and the response duration is very short, less than 0.3 ms.

The damage of explosion load to tunnel was mainly concentrated in a very short time after explosion, which has the characteristics of fast response, large load and short duration.

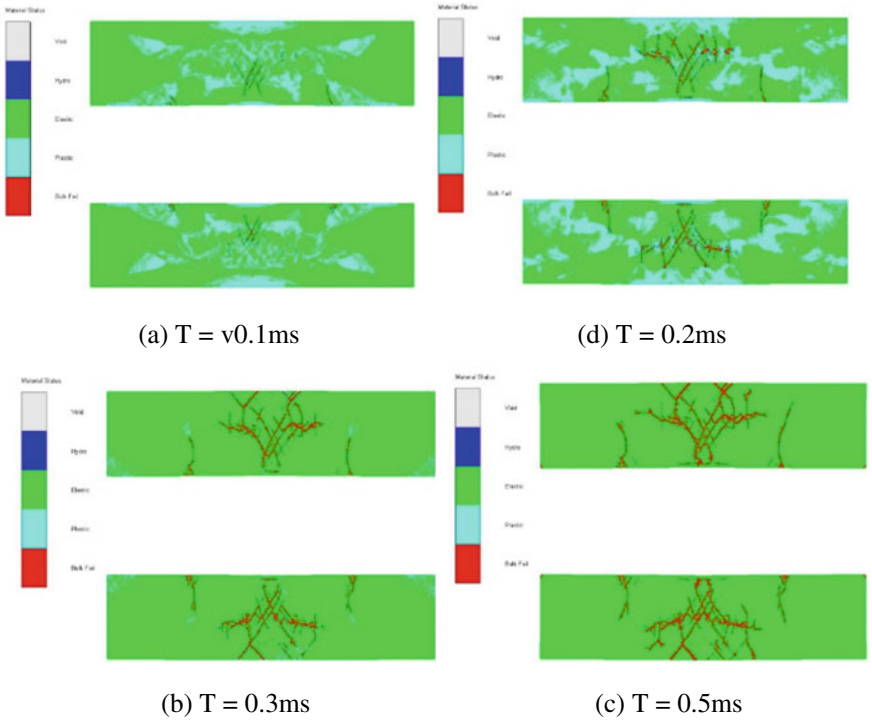

(a) T = v0.1ms (d) T = 0.2ms

(b) T = 0.3ms (c) T = 0.5ms

Fig. 11.4 Rock damage distributing graph after the explosion of burst point 3 in the straight tunnel

11.3.2 L-shaped Tunnel

Figures 11.7 and 11.8 show the stress distributing graph and crack propagation process of rock structure under the load of explosion of burst point 3 in L-shaped tunnel. The stress of the structure was mainly concentrated in the corner. The damage was mainly concentrated in the wall outside the corner, where the tunnel structure was most vulnerable to damage. When T = 0.5 ms and T = 5 ms, the damage degree of the structure was almost the same, which also shows that the damage of the structure was concentrated in 0.5 ms after the explosion, and the time was very short.

Figure 11.9 shows the dynamic response observed at observation points 1–8 after the explosion of burst point 3 in the L-shape tunnel. Observation point 3 was located at the corner of the inner wall, and the maximum stress observed at observation point 3 was 32.31 MPa. During the subsequent structural deformation, there was a residual stress of about 15 MPa. The maximum stress observed at observation points 1 and 2 were 12.77 MPa and 18.47 MPa, and there were multiple peaks gradually decreasing. When the explosive exploded at the corner of the L-shaped tunnel, the inner corner was impacted by the incident wave and the wave reflected from the outer

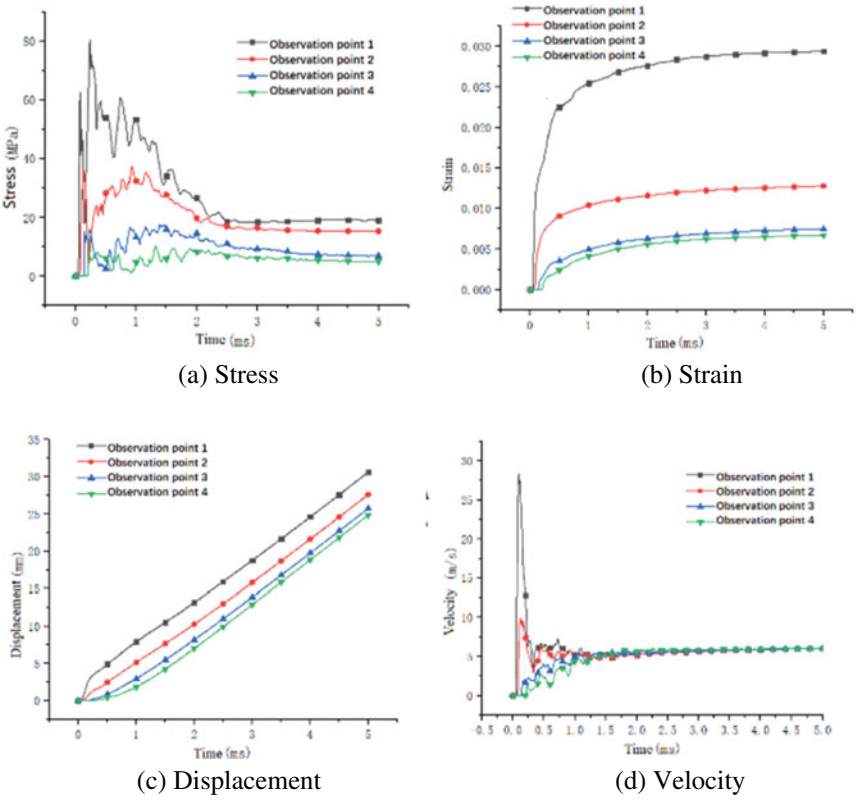

(a) Stress (b) Strain

(c) Displacement (d) Velocity

Fig. 11.5 Dynamic response observed at observation points 1–4 after the explosion of burst point 1 in the straight tunnel

corner to the inner side, and then the shock wave continued to reflect and oscillate in the tunnel.

On the outside of L-shaped tunnel, the maximum stress observed at observation points 4–8 were 17.00, 16.47, 38.57, 72.17 and 91.95 MPa. The closer to the corner, the greater the maximum stress. The maximum strain, displacement and maximum velocity have similar rules. The maximum strain observed at observation point 8 was 0.68, and that at observation point 4–7 were between 0.006 and 0.025, which was far less than that observed at observation point 8. The position of observation point 8 was the most concentrated stress and the most serious damage position.

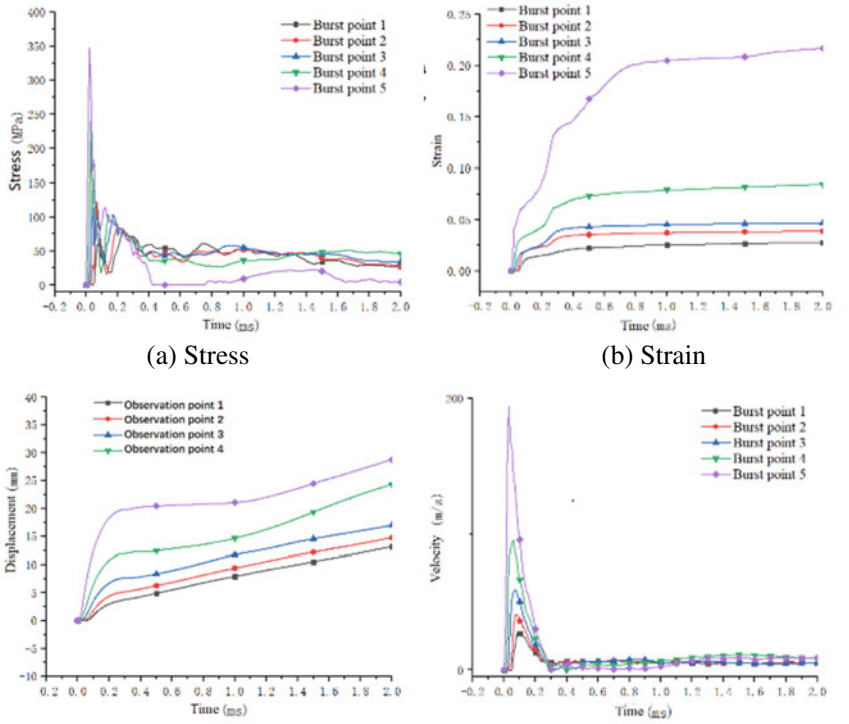

(a) Stress (b) Strain

(c) Displacement (d) Velocity

Fig. 11.6 Dynamic response observed at observation point 1 after the explosion of all burst points in the straight tunnel

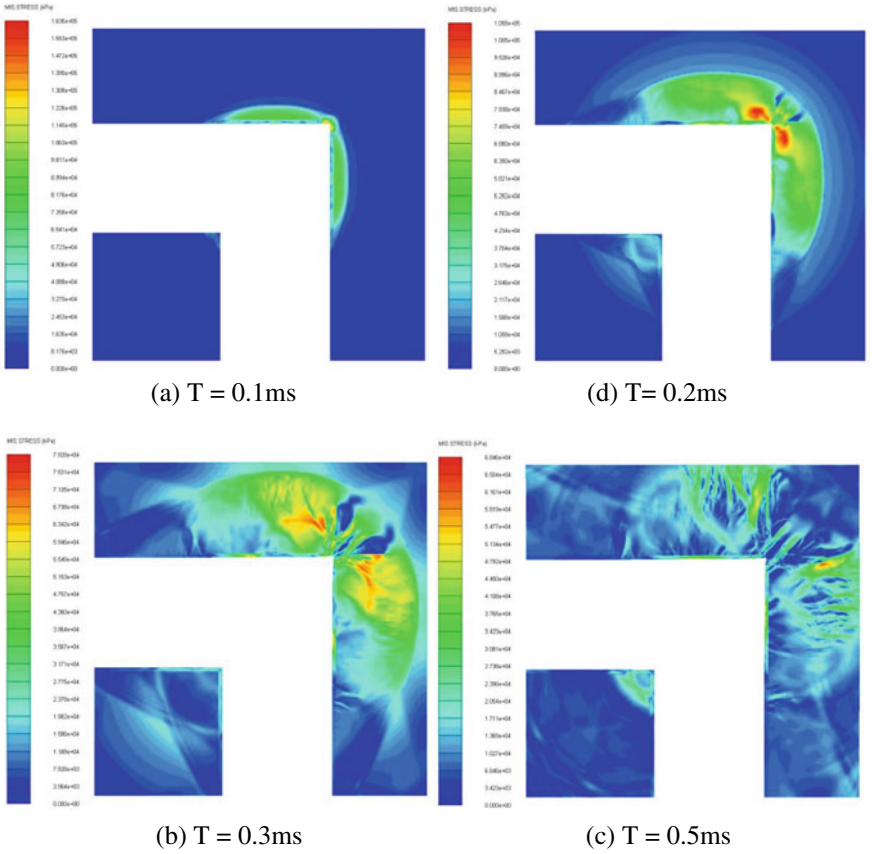

(a) T = 0.1ms (d) T= 0.2ms

(b) T = 0.3ms (c) T = 0.5ms

Fig. 11.7 Stress distributing graph after the explosion of burst point 3 in the L-shape tunnel

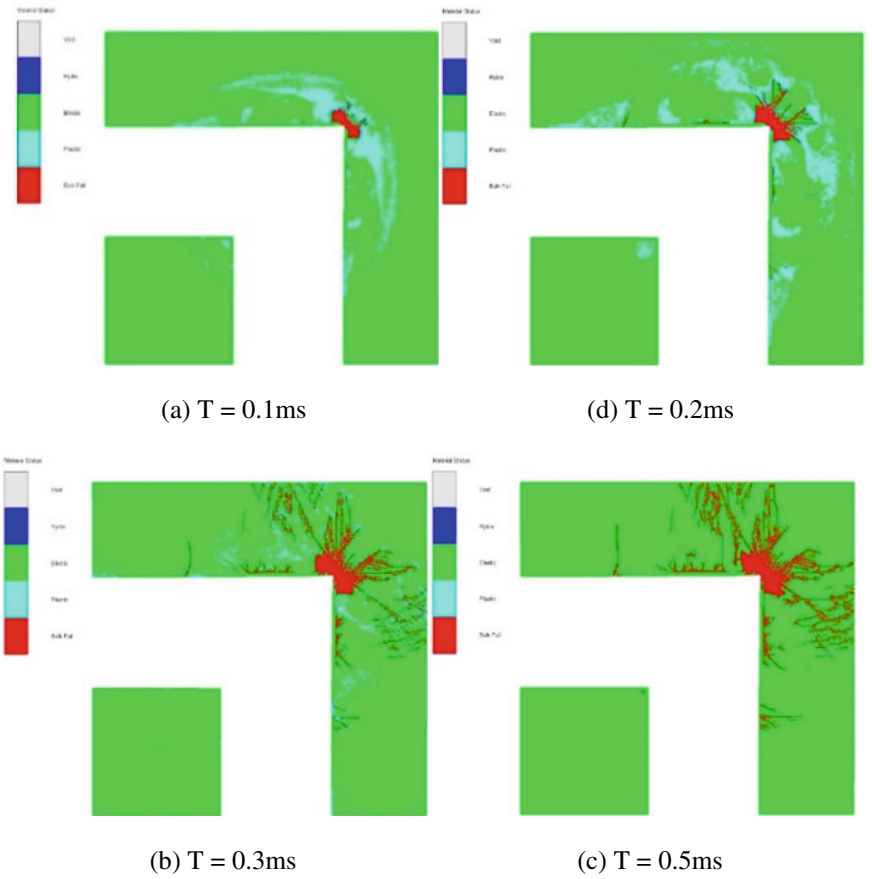

(a) T = 0.1ms (d) T = 0.2ms

(b) T = 0.3ms (c) T = 0.5ms

Fig. 11.8 Rock damage distributing graph after the explosion of burst point 3 in the L-shape tunnel

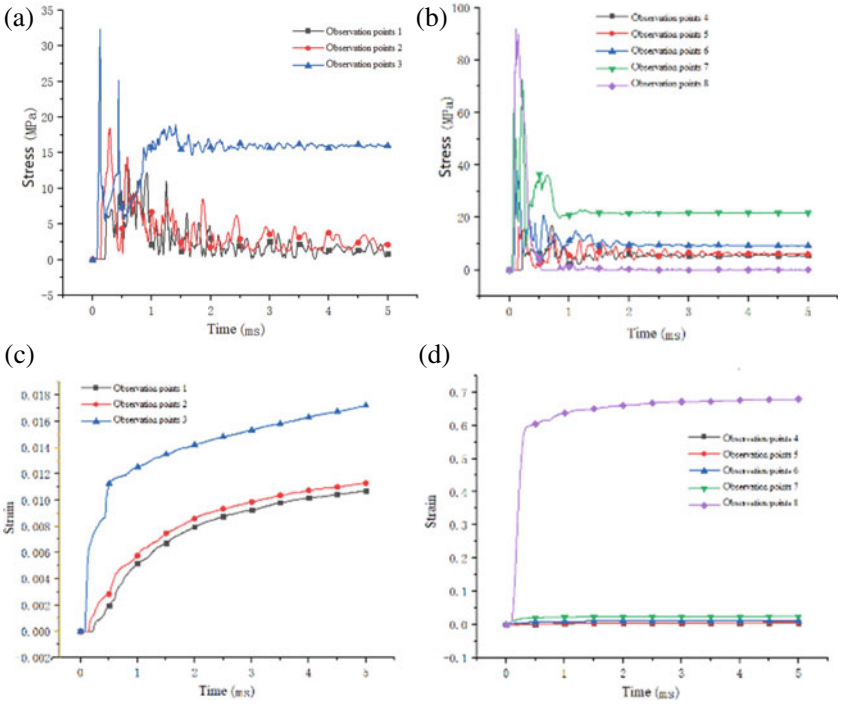

(a) The stress-time curves observed at observation points 1-3

(b) The stress-time curves observed at observation points 4-8

(c) The strain-time curves observed at observation points 1-3

(d) The strain-time curves observed at observation points 4-8

Fig. 11.9 Dynamic response observed at observation points 1–8 after the explosion of burst point 3 in the L-shape tunnel

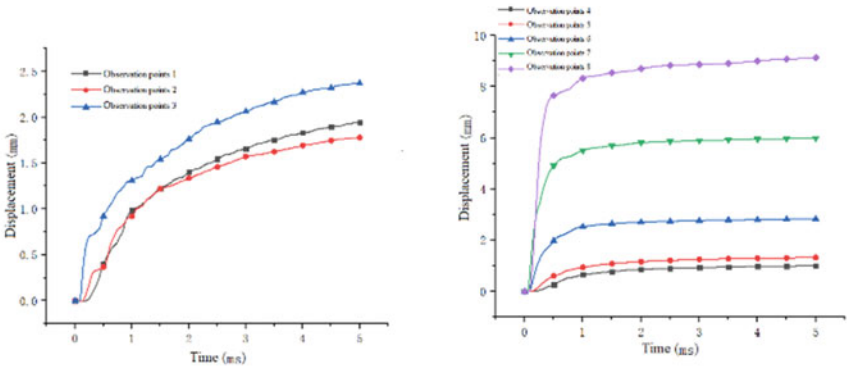

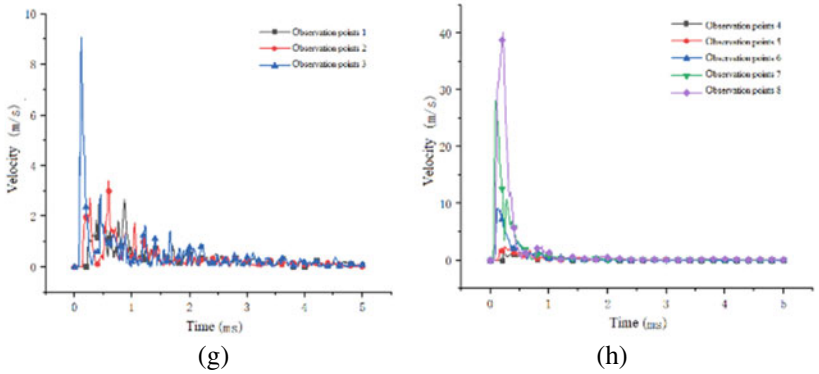

(e) The displacement curves observed at observation points 1-3

(f) The displacement curves observed at observation points 4-8

(g) The velocity-time curves observed at observation points 1-3

(h) The velocity-time curves observed at observation points 4-8

Fig. 11.9 (continued)

Figure 11.10 shows the dynamic response observed at observation points 3 and 8 after the explosion of all burst points in the L-shape tunnel. With the change of burst point 1 to 5, the distance of explosion center to observation point also changed. The maximum stress, strain, displacement and acceleration were negative correlated with the distance from the explosion center. In Fig. 11.10a, the stress observed at observation point 3 decreased rapidly after reaching the highest value (between 20 and 120 MPa), then fluctuated about 1 ms between 0 and 30 MPa, and finally the residual stress stabilized between 10 and 30 MPa. After the stress observed at observation

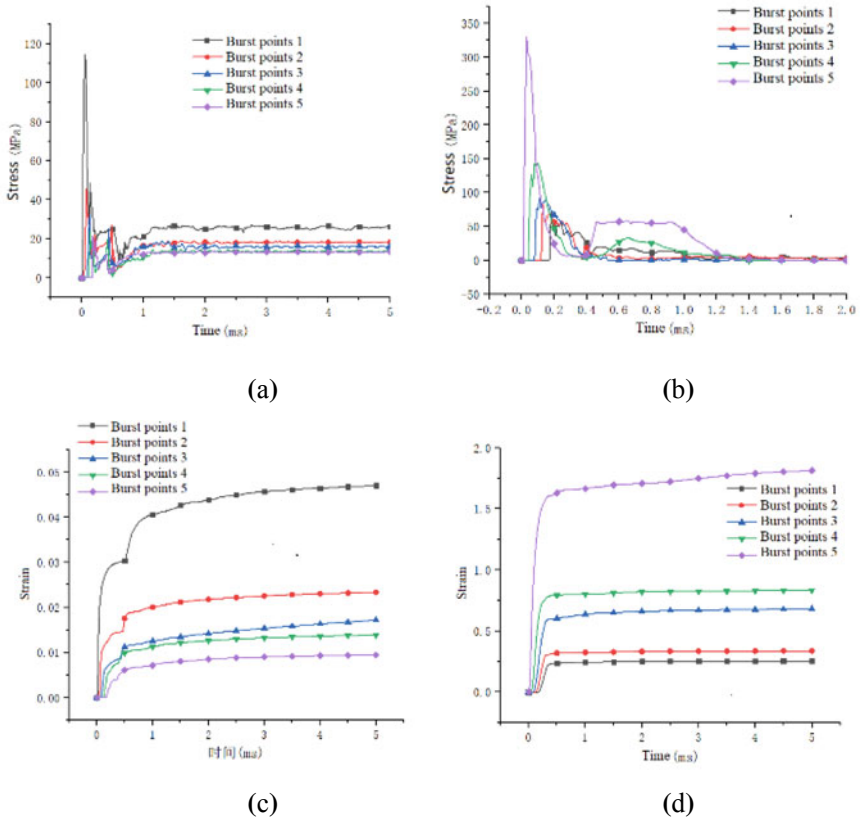

(a) The stress-time curves observed at observation point 3

(b) The stress-time curves observed at observation point 8

(c) The strain-time curves observed at observation point 3

(d) The strain-time curves observed at observation point 8

Fig. 11.10 Dynamic response observed at observation points 3 and 8 after the explosion of all burst points in the L-shape tunnel

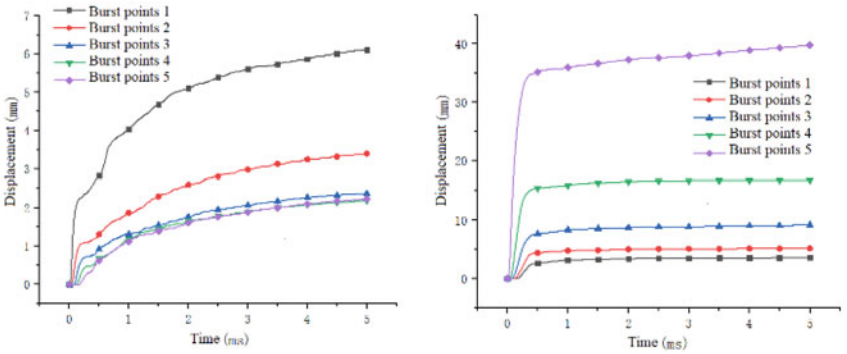

(e)

(f)

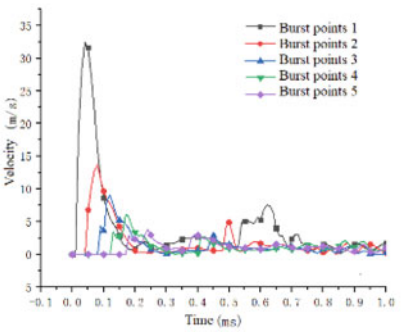

(g)

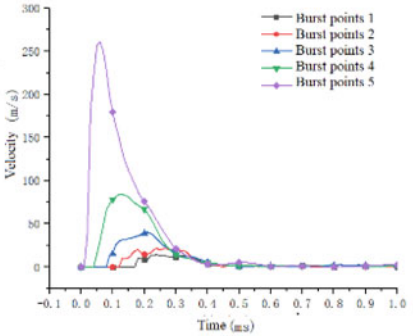

(h)

(e) The displacement curves observed at observation point 3

(f) The displacement curves observed at observation point 8

(g) The velocity-time curves observed at observation point 3

(h) The velocity-time curves observed at observation point 8

Fig. 11.10 (continued)

point 8 reached the highest value (70–330 MPa), it rapidly decreased to 0 MPa in about 0.4 ms, then fluctuated slightly in the stage of 0.4–1.2 ms, and finally returned to 0 MPa. This was because the material had failed and could not longer bear tensile stress. The duration of dynamic response was about 1.2 ms, mainly concentrated in the first 0.4 ms.

Figure 11.11 shows the variation curve of maximum stress and strain observed at observation points 3 and 8. In Fig. 11.11a, the stress change trend observed at observation points 3 was similar with observation points 8. With the increasing of the distance between the burst centers, the maximum stress decreased and the change was gradually gentle, but the maximum value observed at observation point 3 was

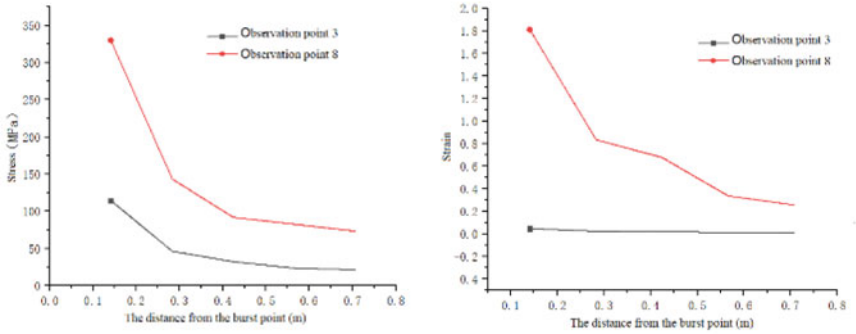

(a) Maximum stress (b) Maximum strain

Fig. 11.11 Variation curve of maximum stress and strain of observation points 3 and 8 with distance between burst points

lower than that at observation point 8. The strain value observed at observation point 8 was large (between 0.256 and 1.81), while the strain observed at observation point 3 was small (between 0.01 and 0.05), and the change was not obvious. Under the load of internal explosion in L-shaped tunnel, the corner position of the outer tunnel was the most stress concentrated position, which was more vulnerable to damage than the inner corner position.

11.3.3 T-shaped Tunnel

Figures 11.12 and 11.13 are the stress distributing graph and crack propagation process of rock structure under the explosion in T-shaped tunnel. After the explosion, the shock wave propagated to the upper wall and corners of the tunnel. The stress was concentrated on the upper wall of T-shaped tunnel. There was also stress concentration on the left and right corners, but it was relatively small. The damage of the structure was mainly in the upper wall. Compared with the straight tunnel, the damage of upper wall in T-shaped tunnel was smaller because the T-shaped tunnel has more bifurcation, which made the explosive energy spread out from the tunnel rapidly.

Figure 11.14 shows the dynamic response observed at all observation points after the explosion of burst point 3 in the L-shape tunnel. On the upper wall of the tunnel, the maximum stress observed at observation points 1–4 were 82.24, 38.88, 16.67 and 14.50 MPa, and the residual stresses were about 23, 17, 6.5 and 4.5 MPa. The maximum stress and residual stress were negatively correlated with the distance from the observation point to the burst point. The maximum strain, displacement and velocity were also the same rule. The response time was about 2 ms.

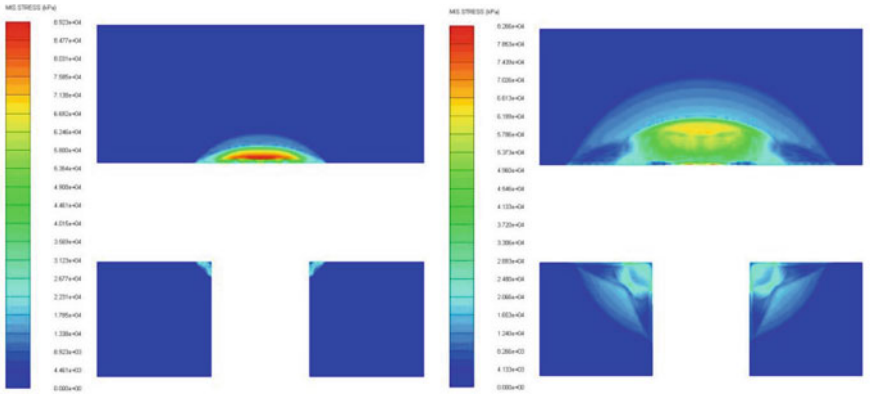

(a) T = 0.1ms (d) T = 0.2ms

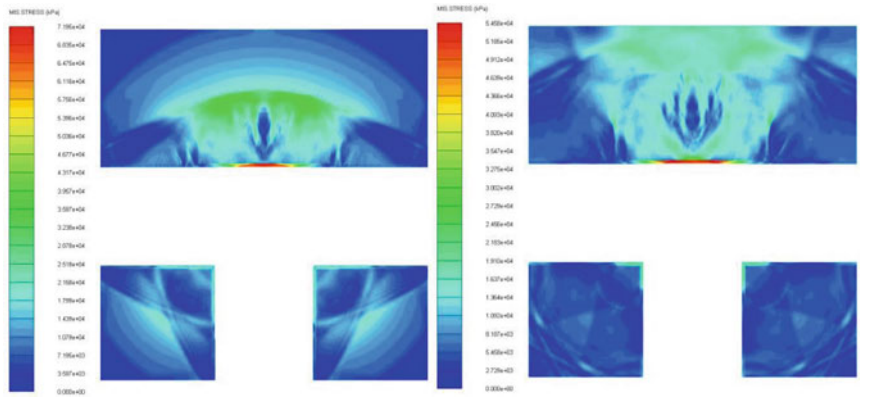

(a) T = 0.1ms (d) T = 0.2ms

Fig. 11.12 Stress distributing graph after the explosion of burst point 3 in the T-shape tunnel

At the lower side of the right corner, the stress observed at observation point 5 rised rapidly to the maximum value of 28.51 MPa after the explosion, then decreased rapidly to 0 MPa, then rised to 28.5 MPa, and then decreased slowly to the residual stress of 16.9 MPa.

The stress curves observed at observation point 6 and 8 were almost the same. After the stress reaches the maximum value of 17.81 and 19.86 MPa, it fluctuated continuously and the peak value decreased gradually. The reason was that the shock wave reflected repeatedly between the inner walls of the tunnel.

The peak value observed at observation points 7 and 9 were about 10 MPa, which decreased slowly and fluctuated continuously. In the lower right side of the tunnel wall, the farther away from the burst point, the smaller the maximum stress, strain, displacement and velocity. And the residual stress was mainly concentrated in the

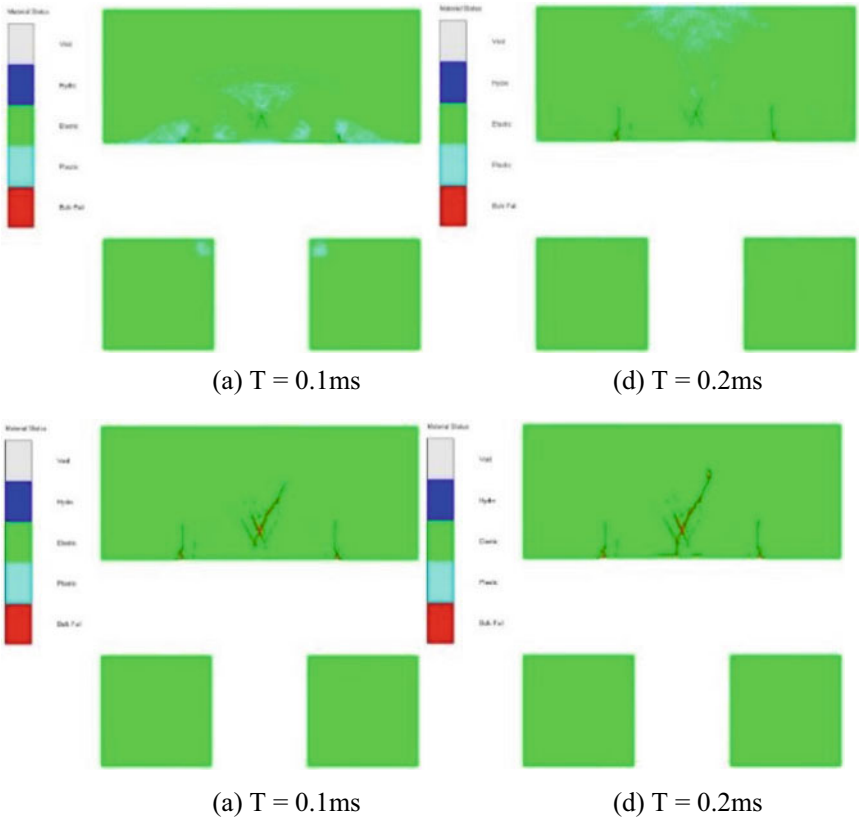

Fig. 11.13 Rock damage distributing graph after the explosion of burst point 3 in the T-shape tunnel

corner of the tunnel. Compared with the straight tunnel and L-shape tunnel, the dynamic response time was longer which reached 2–3 ms.

Figure 11.15 shows the dynamic response observed at observation points 1 and 5 at different burst points. At explosion point 1, the maximum stress reached 354.5 MPa, and then gradually decreased to 0 MPa, which indicated that the element had failed and could no longer bear tensile stress or shear stress. For other explosion points, there was residual stress observed at observation points 1, which was 20–40 MPa. The maximum stress observed at observation point 5 increased from 23.6 to 80.6 MPa, and the maximum strain, displacement and acceleration also increased gradually. The center of the upper wall and the left and right corners were vulnerable points, and the load was positively correlated with the distance between the explosion centers. Compared with the straight tunnel and L-shaped tunnel, the response time is longer, reaching 2–3 ms.

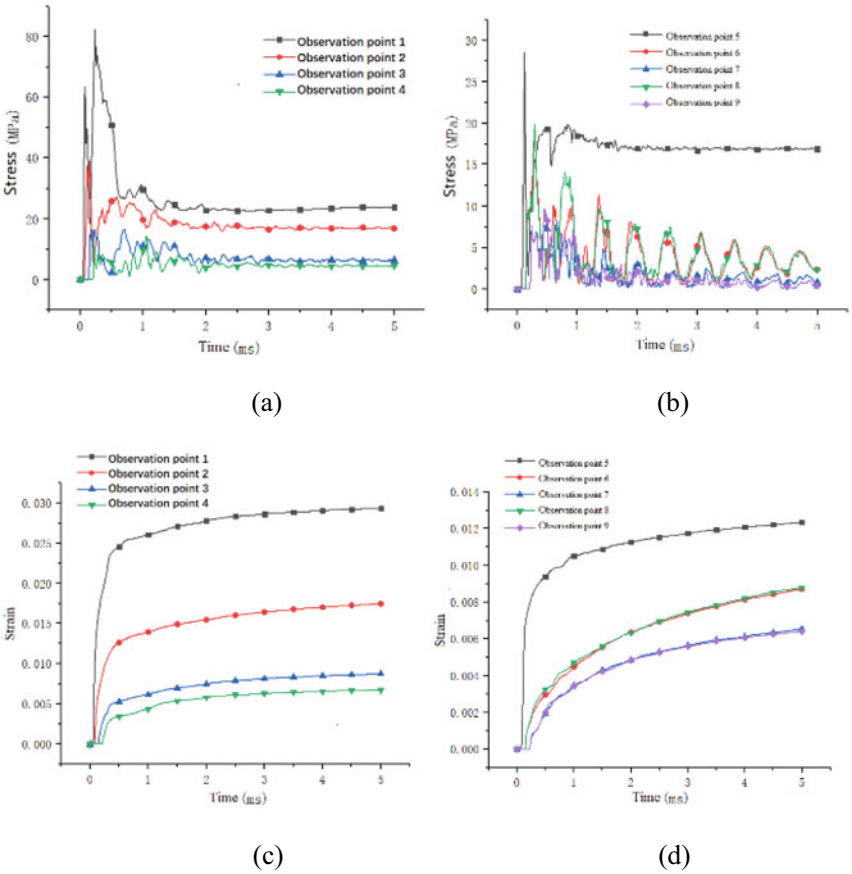

(a) The stress-time curves observed at observation points 1-4

(b) The stress-time curves observed at observation points 5-8

(c) The strain-time curves observed at observation points 1-4

(d) The strain-time curves observed at observation points 5-8

Fig. 11.14 Dynamic response observed at observation points 1–8 after the explosion of burst point 3 in the T-shape tunnel

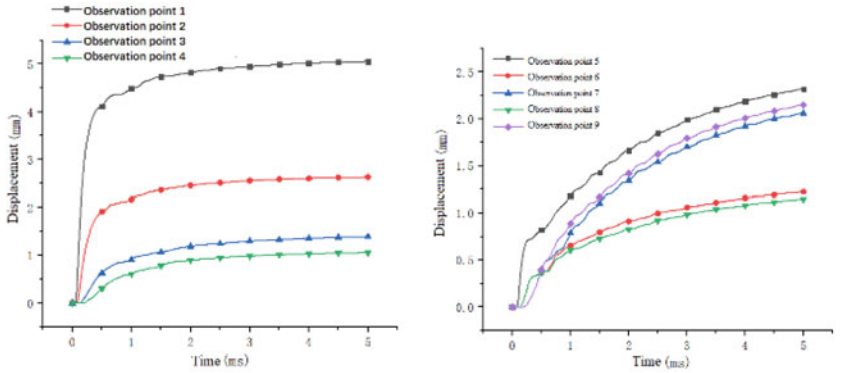

(e) (f)

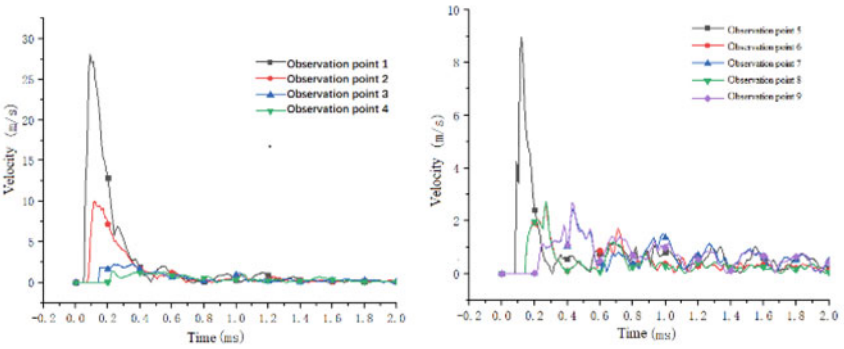

(g) (h)

(e) The displacement curves observed at observation points 1-4

(f) The displacement curves observed at observation points 5-8

(g) The velocity-time curves observed at observation points 1-4

(h) The velocity-time curves observed at observation points 5-8

Fig. 11.14 (continued)

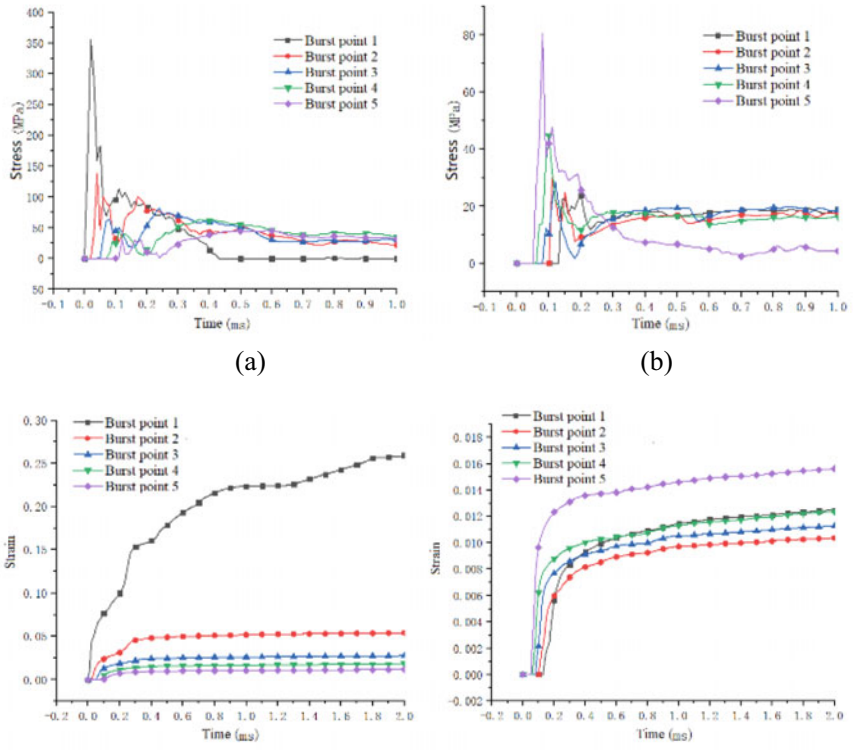

(a) The stress-time curves observed at observation point 1

(b) The stress-time curves observed at observation point 5

(c) The strain-time curves observed at observation point 1

(d) The strain-time curves observed at observation point 5

Fig. 11.15 Dynamic response observed at observation points 1 and 5 after the explosion of all burst points in the T-shape tunnel

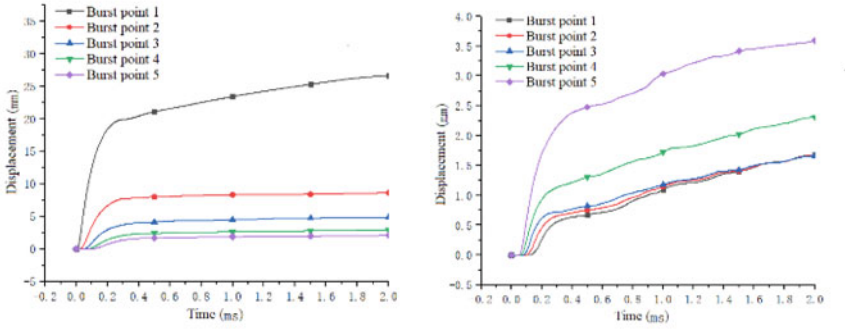

(e)

(f)

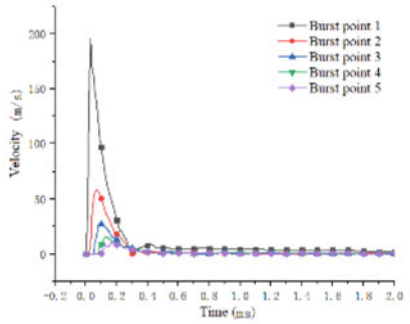

(g)

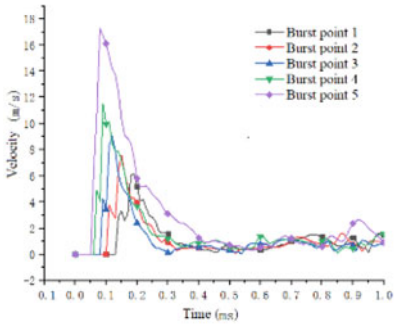

(h)

(e) The displacement curves observed at observation point 3

(f) The displacement curves observed at observation point 8

(g) The velocity-time curves observed at observation point 1

(h) The velocity-time curves observed at observation point 5

Fig. 11.15 (continued)

11.4 Conclusion

In this paper, the physical model of the explosion structure in the tunnel was established, the suitable material constitutive model and parameters were selected. The dynamic response of the tunnel structure with different shapes under the explosion load was numerically simulated, and the failure forms of tunnel and rock structure were analyzed.

The stress of concrete tunnel and rock increases rapidly under explosion load. Concrete and rock materials will have elastic strain and plastic strain. When the stress exceeds the maximum tensile stress that the material can bear, the material will fail. After failure, the material can no longer bear tensile stress or shear stress, forming cracks. With the propagation of stress, the cracks gradually expand, and the main generation and propagation time of cracks is 0–0.5 ms.

The damage of explosion load to tunnel is mainly concentrated in a very short time after explosion, which has the characteristics of fast response (0.003–0.05 ms, reaching microsecond level), large load (from tens to hundreds MPa), short duration (0.3–3 ms).

Based on the 5 kg spherical COMP B used in this paper, when the distance between the burst point and the wall is less than 0.1 m, the wall structure will fail completely; In the L-shaped tunnel, stress concentration occurs at the outer corner of the structure, and the structure with a distance of 0.3 m also fails completely; On the contrary, in the inner corner, there is no complete failure of the material. The center of the upper wall and the left and right corners of the T-shaped tunnel are the most concentrated parts to bear the explosion load, and the center of the upper wall is the most vulnerable part.

References

1. X. Ren, Q. Zhang, Y. Xue, Experimental study on propagation velocity model of blast wave of explosive B at tunnel entrance. J. Vibr. Shock **31**(7) (2012)
2. Z. Guo, C. Wang, X. Zhang, et al., Study on Multiaxial Strength Test and Failure Criterion of Concrete (Tsinghua University Press, Beijing, 2003)
3. L.I. Hongchao et al., Study on parameters determination of marble RHT model. Trans. Beijing Inst. Technol. **37**(8), 801–806 (2017)
4. B.M. Luccioni, R.D. Ambrosini, R.F. Danesi, Analysis of building collapse under blast loads. Eng. Struct. **26**(1), 63–71 (2004)
5. J. Henrych, *The Dynamics of Explosion and Its Use* (Elsevier Scientific Publishing Company, Amsterdam, 1979), pp. 178–181
6. J.R. Britt, Attenuation of short duration blast in entranceways and tunnels, in *Proceeding of the 2nd Symposium on the Interaction of Non-nuclear Munitions with Structures, Panama City Beach, Florida* (1985), pp. 466–471
7. A.M. Benselama, M.J. William-Louis, F. Monnoyer et al., A numerical study of the evolution of the blast wave shape in tunnels. J. Hazard. Mater. **181**(1–3), 609–616 (2010)
8. D. Uystepruyst, F. Monnoyer, A numerical study of the evolution of the blast wave shape in 1rectangular tunnels. J. Loss Prev. Process Ind. **34**, 225–231 (2015)

9. A.C. Smith, M.J. Sapko, Detonation wave propagation in underground mine entries. J. Mine Ventilat. Soc. South Africa, 2005 Jan/Mar, 20–25.
10. K. Yang, X. Yang, Propagation law of chemical explosion shock wave in tunnel. Explos. Shock Waves **23**(1), 1.37–1.41 (2003)
11. W. Pang, X. He, M. Li, H. Ren, Experimental study on travel time of air shock wave in tunnel. Explos. Shock Waves **23**(6), 11 (2003)
12. W.E. Baker, *Explosions in air* (University of Texas Press, Austin, 1973), pp. 7–15
13. US Army Engineer Waterways Experiment Station, Department of the Army. Fundamental of protective design for conventional weapon. Vicksburg (1986)
14. C.R. Welch, In-tunnel air blast engineering model for internal and external detonations, in *Proceeding of the 8th International Symposium on Interaction of the Effects of Munitions with Structures, Mclean, Virginia*, 195–208 (1997)
15. G. Scheklinski, Blast in tunnels and rooms from cylindrical HE-charges outside the tunnel entrance, in *Douglass H M.Proceedings of the 6th Symposium on the International of Non-nuclear Munition with Structures*, Panama City Beach, Florida (1993), pp. 68–73
16. W. Fondaw, Grant. (1993). *Mitigation of Shock Waves in a Cylindrical Tunnel by Foam*, 116
17. J.K. Yi, H. Shen, K.B. Yan, B. Bing, A review of numerical study on explosion and shock wave resistance of metal foam material. Adv. Mater. Res. **936**, 2024–2029 (2014)
18. M.D. Goel, P. Altenhofer, V.A. Matsagar, A.K. Gupta, C.Mundt, S. Marburg, Interaction of a shock wave with a closed cell aluminum metal foam. Combust. Explos. Shock Waves 51(3) (2015)
19. M. Nusser, A. Hermann, V. Senner, Corrigendum to 'artificial knee joint and ski load simulator for the evaluation of knee braces and ski bindings', in *11th conference of the International Sports Engineering Association, ISEA 2016, Procedia Engineering*, vol. 147 (2016), pp. 220–227
20. J. Lajeunesse, Implications of heterogeneity in the shock wave propagation of dynamically shocked materials. Dissert. Theses Gradw **9**, 235–238 (2015)
21. D.P.D.P. Mondal, S. Das, Effect of thickening agent and foaming agent on the micro-architecture and deformation response of closed cell aluminum foam. Einfluss des Dickungs- und Treibmittels auf die Mikrostruktur und das Deformationsverhalten von geschlossenzelligem Aluminiumschaum. Materialwissenschaft und Werkstofftechnik **41**(5) (2010)
22. T. Krauthammer, C.K. Ku, *Backfill Effects on Partially Buried Shelter Response Under Close in Conventional Explosions* (Computational Mechanics Publications LTD, Madrid, 1994), pp. 349–356
23. H.L. Brode, Blast wave from a spherical charge. Phys. Fluids **2**(2), 217–229 (1959)
24. J. Henrych, G.R. Abrahamson, *The Dynamics of Explosion and Its Use* (Academia, 1979)
25. W.E. Baker, *Explosion Hazards and Evaluation* (Elsevier Scientific Pub. Co., 1983)
26. X.H. Mao, Dynamic response of the compound structure of foam aluminum core composite sandwich material to the shock wave of gas explosion. Adv. Mater. Res. 2384 (2013)
27. P.D. Smith, P. Vismeg, L.C. Teo et al., Blast wave transmission along rough-walled tunnels. Int. J. Impact Eng. **21**(6), 419–432 (1998)
28. H. Guozhen, Y. Zan, Numerical Simulation Study on the Propagation of Shock Wave in the Corridor. Structural Engineering Committee of Chinese society of mechanics, Xi'an University of architecture and technology, editorial board of engineering mechanics, in *Proceedings of the 27th National Conference on Structural Engineering*, vol. II. Structural Engineering Committee of Chinese Society of Mechanics, Xi'an University of Architecture and Technology, editorial board of Engineering Mechanics. J. Eng. Mech. (2018)
29. Z. Yuetang, D. Xiaopeng, Y. Yijun, C. Cheng, Methods for improving the resistance of flatbed protective doorframe wall under intensive impact loading. Explos. Shock Waves **37**(03), 487–495 (2017)
30. K. Qu, Y. Yan, Y. Liu, X. Ning, Z. Li, Comparative study on propagation rules of explosive shock-wave in long straight and complex tunnel. Chin. J. Appl. Mech. **28**(04), 434–438+457 (2011)